Cylindrically shaped zinc-blende semiconductor quantum dots do not have cylindrical symmetry: Atomistic symmetry, atomic relaxation, and piezoelectric effects

Gabriel Bester and Alex Zunger
National Renewable Energy Laboratory, Golden, Colorado 80401, USA
(Received 1 April 2004; published 14 January 2005)

Self-assembled quantum dots are often modeled by continuum models (effective mass or $\mathbf{k}\cdot\mathbf{p}$) that assume the symmetry of the dot to be that of its overall geometric shape. Lens-shaped or conical dots are thus assumed to have continuous cylindrical symmetry $C_{\infty v}$, whereas pyramidal dots are assumed to have C_{4v} symmetry. However, considering that the III–V dots are made of atoms arranged on the (relaxed) positions of a zinc-blende lattice, one would expect the highest possible symmetry in these structures to be C_{2v}. In this symmetry group all states are singly degenerate and there are no *a priori* reason to expect, e.g., the electron *P* states (usually the second and third electron levels of dominant orbital *P* character) to be degenerate. Continuum models, however, predict these states to be energetically degenerate unless an irregular shape is postulated. We show that, in fact, the true (atomistic) symmetry of the dots is revealed when the effects of (i) interfacial symmetry, (ii) atomistic strain, and (iii) piezoelectricity are taken into account. We quantify the contributions of each of these effects separately by calculating the splitting of electron *P* levels for different dot shapes at different levels of theory. We find that for an ideal square-based pyramidal InAs/GaAs dot the interfacial symmetry of the unrelaxed dot splits the *P* level by 3.9 meV, atomistic relaxation adds a splitting of 18.3 meV (zero if continuum elasticity is used to calculate strain) and piezoelectricity reduces the splitting by −8.4 meV, for a total splitting of 13.8 meV. We further show that the atomistic effects (i) and (ii) favor an orientation of the electron wave functions along the $[1\bar{1}0]$ direction while effect (iii) favors the [110] direction. Whereas effects (i) + (ii) prevail for a pyramidal dot, for a lens shaped dot, effect (iii) is dominant. We show that the 8–band $\mathbf{k}\cdot\mathbf{p}$ method, applied to pyramidal InAs/GaAs dots describes incorrectly the splitting and order of *P* levels (–9 meV instead of 14 meV splitting) and yields the orientation [110] instead of $[1\bar{1}0]$.

DOI: 10.1103/PhysRevB.71.045318 PACS number(s): 73.21.La, 71.15.−m, 73.22.Dj

I. INTRODUCTION: WHY DO DOTS HAVE LOWER SYMMETRIES THAN SUGGESTED BY THEIR SHAPE ALONE

Current vapor-phase Stranski-Krastanov growth techniques for self-assembled In-GaAs/GaAs quantum dots tend to produce nanostructures with *cylindrical-like* shape symmetry, e.g. disks, truncated cones, lenses, or pyramids.[1–6] Spectroscopic studies of such dots reveal polarized transitions between confined hole and confined electron levels. Theoretical modeling used to understand the observed spectroscopic transitions and their polarizations need to assume the symmetry and shape of such dots. The vast majority of the calculations performed on quantum dots (see Refs. 7 and 8) use a confinement potential which is assumed to have just the *shape symmetry* of the nanostructure. This is the approach used in the conventional $\mathbf{k}\cdot\mathbf{p}$[9–11] method, in the effective mass approximation (EMA),[12,13] in the EMA followed by a local density approximation treatment EMA-LDA [14] and in the path integral quantum Monte Carlo-EMA[15] method. In such continuum-like descriptions of the potential, a quantum dot with the overall shape of a square-based pyramid is assumed to have C_{4v} symmetry, while quantum dots with an overall disk, truncated cone or lens shape are assumed to have cylindrical symmetry $C_{\infty v}$. With such assumed symmetries the dots have twofold degenerate *P* and *D* levels with no optical polarization anisotropy in the (001)-plane. These symmetries carry over to the description of many-particle excitonic states. However, in general, the true symmetry of even an *ideally shaped* quantum dot is lower than the shape symmetry. This is a consequence of the atomistic nature of the structure that lowers the symmetry of the earlier mentioned quantum dots to C_{2v}. In this symmetry group no degeneracy can be expected *a priori* and polarization anisotropies are possible, and indeed observed.[16–19] However, to explain these within continuum approaches, it is customary to postulate some unspecified geometric irregularity of the dots. This is not necessary if the atomistic symmetry is considered. There are three reasons for the symmetry lowering relative to the naive expectations based on shape alone. *First*, the interface between the dot material (InAs) and the barrier material (GaAs) lowers the symmetry (even in the absence of strain) since the interface plane is not necessarily a reflection plane. This creates a short-range interfacial potential. *Second*, atomic relaxations due to the atomic size difference between Ga and In respond to the earlier noted short-range potential asymmetry, creating a displacement field that enhances the magnitude of the asymmetry. This component is not captured if the relaxation is performed using classic harmonic continuum-elasticity approach[20] as the latter "sees" only the shape. Instead, atomistic elasticity[21] is needed. *Finally*, a long-ranged piezoelectric field can develop in response to the displacement field, as recognized by Grundmann *et al.*,[22] contributing a distinct term to the total potential. The total potential, and thus the splitting of *P* and *D* confined levels has contributions from (i) interfacial atomic symmetry lowering, (ii) atomic relaxation, and (iii) the piezoelectric field. Note that

such symmetry lowering exists already for ideally shaped dots, e.g., perfect square-based pyramid with zincblende structure. The classic effective-mass and $\mathbf{k}\cdot\mathbf{p}$ treatment of nanostructures[9,11] neglects all three effects giving rise to unsplit P and D states and unpolarized inter- and intraband transitions. A possible cure to the lack of polarization anisotropies and simplified photoluminescence spectra of the continuum methods was given in the works of Stier, Grundmann, and Bimberg,[22–24] Pryor,[25] and Hackenbuchner *et al.*[26] where the piezoelectric potential has been added as an external field to the classical $\mathbf{k}\cdot\mathbf{p}$ Hamiltonian. The strain field, on the other hand, has been included atomistically using the valence force field (VFF) method[27] in the $\mathbf{k}\cdot\mathbf{p}$ framework[23,24,26,28,29] as described, e.g., by Bahder.[30] However, the inversion symmetry breaking introduced by the atomistic strain field (via VFF) is not well represented using the underlying assumption of slowly varying potentials (and envelope functions) and parabolic bands in $\mathbf{k}\cdot\mathbf{p}$. Stier *et al.*[24,31] and Jiang *et al.*[28] report negligible splittings of the electron P states without piezoelectricity. More generally, this observation leeds to the conclusion that the discrepancies described in Pryor *et al.*[21] between the atomistic and the continuum descriptions of strain cannot be properly accounted by $\mathbf{k}\cdot\mathbf{p}$ methods. The need for an atomistic basis set as, e.g., used in the empirical pseudopotential approach[32] or in tight-binding calculations[33–37] becomes apparent. In the present contribution we perform calculations that include on the same atomistic footing the effects of dot interface, atomic relaxation, and piezoelectricity. This methodology is used to isolate the different effects that reveal the true atomistic C_{2v} symmetry of quantum dots. We start by presenting the methodology emphasizing the addition of the piezoelectric field to the well established empirical pseudopotential method. We then isolate three distinct effects that reveal the atomistic nature of the nanostructure and quantify their importance.

II. THEORETICAL METHODS

We solve the single-particle Schrödinger equation for the Hamiltonian

$$\hat{H} = -\frac{\beta}{2}\nabla^2 + \sum_{n\alpha}[v_\alpha(\mathbf{r}-\mathbf{R}_n) + \hat{\mathrm{v}}_\alpha^{SO}] + V_{\mathrm{piezo}}(\mathbf{r}) \qquad (1)$$

which includes a kinetic energy term, a pseudopotential part (second and third term), and a piezoelectric potential part (last term). The screened atomic pseudopotentials v_α (with α=Ga,In,As,…) are centered around the locally relaxed atomic positions $\mathbf{R}_n$. The atomic relaxation is performed using the valence force field method to minimize the strain energy[32,38]. The empirical atomic pseudopotentials v_α are fit in reciprocal space to accurately reproduce the electronic band structure, the electron effective mass, the heavy hole effective masses along the [100] and [111] directions, the light hole effective mass along the [100] direction, the spin-orbit splittings at the Γ_{15v} and L_{1v} points, the hydrostatic and biaxial deformation potentials.[38] The detail of the fitting procedure and the obtained parameters are reported in Ref. 38. The same parameters as in Ref. 38 have been used in this work. The empirical pseudopotentials $v_\alpha(\mathbf{G})$ has an explicit dependence on the local hydrostatic strain, $\mathbf{T}r(\epsilon)$. This dependence is crucial to obtain a correct description of the volume deformation potential.[38,39] The spin-orbit interaction $\hat{\mathrm{v}}_\alpha^{SO}$ is implemented in $\mathbf{G}$ space as described in Ref. 38. The pseudopotentials v_α constructed that way do not include the effect of piezoelectricity which represent the formation of a polarization field due to the presence of off-diagonal components of the strain tensor. This field is typically too long ranged to be included in the atomistic pseudopotential v_α and is not represented in any of the target values used to fit $v_\alpha(\mathbf{G})$. The piezoelectric potential must therefore be incorporated as an external additional potential.

Piezoelectricity is given, in the linear regime, by a tensor of third rank, e_{ijk}, that connects the strain tensor ϵ_{ij} and the polarization[40] P:

$$P_i = \sum_{ijk} e_{ijk}\epsilon_{jk}. \qquad (2)$$

In the common matrix representation it is written as

$$\begin{pmatrix} P_x \\ P_y \\ P_z \end{pmatrix} = \begin{pmatrix} e_{11} & e_{12} & e_{13} & e_{14} & e_{15} & e_{16} \\ e_{21} & e_{22} & e_{23} & e_{24} & e_{25} & e_{26} \\ e_{31} & e_{32} & e_{33} & e_{34} & e_{35} & e_{36} \end{pmatrix} \begin{pmatrix} \epsilon_{xx} \\ \epsilon_{yy} \\ \epsilon_{zz} \\ \epsilon_{yz}+\epsilon_{zy} \\ \epsilon_{zx}+\epsilon_{xz} \\ \epsilon_{xy}+\epsilon_{yx} \end{pmatrix}. \qquad (3)$$

For crystal structures with inversion symmetry, $\mathbf{P}=-\mathbf{P}$ so $e_{ij}\equiv 0$ for all i, j. For crystals with zinc-blende structure, all components of e_{ij} are zero except $e_{14}=e_{25}=e_{36}$, leading to the simple relationship

$$\begin{pmatrix} P_x \\ P_y \\ P_z \end{pmatrix} = \begin{pmatrix} e_{14} & 0 & 0 \\ 0 & e_{14} & 0 \\ 0 & 0 & e_{14} \end{pmatrix} \begin{pmatrix} \epsilon_{yz}+\epsilon_{zy} \\ \epsilon_{zx}+\epsilon_{xz} \\ \epsilon_{xy}+\epsilon_{yx} \end{pmatrix}, \qquad (4)$$

where only off-diagonal components of the strain tensor remain. The strain tensor is a function of position and we calculate it for each cation position in the crystal. The local polarization, however, cannot be defined on an arbitrarily small region of space,[41] but only on a scale that exceeds the localization of the maximally localized Wannier functions.[42] For GaAs and InAs we conclude that it is only meaningful to consider spacial variations of the polarization on a scale larger than the anion-cation distance, and in praxis we average the strain tensor over eight atom cells. The piezoelectric constant is therefore position dependent. For regions of space where all three atom types (In,Ga,As) are present, we calculate the average over the bulk values of InAs[43] ($-0.045\ \mathrm{C/m^2}$) and GaAs[43] ($-0.16\ \mathrm{C/m^2}$) weighted by the number of In and Ga atoms in each eight atom cell. The piezoelectric charge is obtained from the divergence of the polarization

$$\rho_{\text{piezo}}(\mathbf{r}) = -\nabla \cdot \mathbf{P} = -\nabla \cdot \begin{Bmatrix} e_{14}(\mathbf{r})\{\epsilon_{yz}(\mathbf{r}) + \epsilon_{zy}(\mathbf{r})\} \\ e_{14}(\mathbf{r})\{\epsilon_{zx}(\mathbf{r}) + \epsilon_{xz}(\mathbf{r})\} \\ e_{14}(\mathbf{r})\{\epsilon_{xy}(\mathbf{r}) + \epsilon_{yx}(\mathbf{r})\} \end{Bmatrix}. \tag{5}$$

The divergence is calculated using a piecewise polynomial function to represent the polarization data points.[44]

In the last step the piezoelectric potential V_{piezo} is obtained from the Poisson equation

$$\rho_{\text{piezo}}(\mathbf{r}) = \epsilon_0 \nabla \cdot \{\epsilon_s(\mathbf{r}) \nabla V_{\text{piezo}}(\mathbf{r})\}. \tag{6}$$

The piezoelectric density ρ_{piezo} is thereby expanded in multipoles up to a certain angular momentum to obtain the accurate boundary conditions for the long-ranged potential. The Poisson equation is then solved using a conjugate gradient algorithm finding the piezopotential $V_{\text{piezo}}(\mathbf{r})$. Particular care has been taken for the numerical differentiation where basic finite difference methods have been tested against polynomial interpolations. While the results of both approaches are in excellent agreement, the convergence of the conjugate gradient algorithm is most stable with polynomials of third order.[44] For grid sizes of $80\times80\times80$ the result is usually obtained in a dozen iterations within a few minutes of computational time on a standard personal computer.

Once the total potential $\Sigma_{n\alpha}[v_\alpha(\mathbf{r}-\mathbf{R}_n)+\hat{v}_\alpha^{SO}]+V_{\text{piezo}}(\mathbf{r})$ is defined, the basis set has to be chosen. The single-particle dot wave functions are expanded in terms of strain-dependent Bloch functions $\psi_i=\Sigma A_{n,\mathbf{k}}\varphi_{n,\mathbf{k}}(r)$ of band index n and wave vector $\mathbf{k}$ of the underlying bulk solids. In this "linear combination of bulk bands" approach,[45] basis functions are obtained throughout the Brillouin zone and differ in this respect from the $\mathbf{k}\cdot\mathbf{p}$ method. This results in a far greater[46] variational accuracy, and incorporates naturally both intervalley (e.g., $\Gamma-X-L$) and multiband (various n's) couplings. The ladder of electron (hole) single-particle states will be denoted as $e_0,e_1,e_2,\ldots$ $(h_0,h_1,h_2,\ldots)$ for ground state, first excited state, etc.

III. EFFECTS REVEALING THE ATOMISTIC SYMMETRY OF THE NANOSTRUCTURE

In this section we will discuss the three distinct physical effects responsible for the lowering of the symmetry, starting from the continuum-like symmetry and progressing to the true atomistic symmetry. In order to quantify the importance of these effects, we will present specific results on the splitting of the single-particle electron P states. In a continuum-like description these states are exactly degenerate and their wave functions are isotropic in the (001) plane. On the other hand, the fully atomistic description of a cylindrical, lens shaped or pyramidal dot yields split P states with well defined wave function orientation, either along the [110] or the $[1\bar{1}0]$ directions. We will report on the energetic splitting $\Delta E=\varepsilon_{[110]}-\varepsilon_{[1\bar{1}0]}$ where $\varepsilon_{[110]}$ $(\varepsilon_{[1\bar{1}0]})$ is the single particle energy of the electron state oriented along the [110] $([1\bar{1}0])$ direction for different dot shapes and sizes, given in Fig. 1.

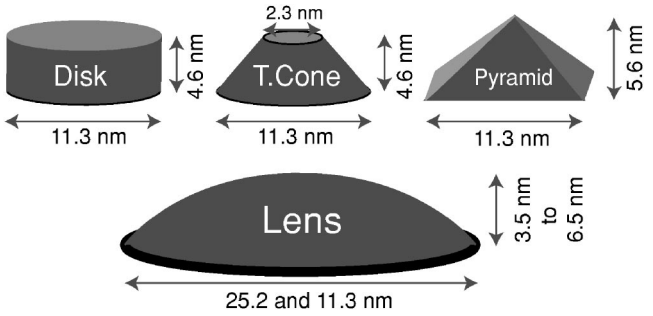

FIG. 1. Shapes and sizes of InAs/GaAs dots considered. Disk, truncated cone (T.Cone), pyramid, and lens.

We consider a set of dots with a common base dimension of 11.3 nm and different shapes and sizes: a disk with 4.6 nm height, a truncated cone with a top base of 2.3 nm, and a height of 4.6 nm, a pyramid with a height of 5.6 nm ({101} side facets), a lens with 4.6 nm height. In addition we calculated sizes that are more realistic,[3,4] namely a set of lenses with 25.2 nm base and four different heights (3.5, 5.0, 5.5, 6.5 nm). To isolate the physical factors responsible for level splitting and wave function anisotropy of dots with ideal shape symmetry we distinguish four levels of theory, starting from the simplest. While there are other ways of separating the various effects, the partitioning below is a convenient way to isolate the main physical effects of chemical symmetry, short-ranged relaxation and long-ranged strain fields.

Level 1: The symmetry of the nanostructure is taken as the shape symmetry; so a pyramid is assumed to have C_{4v} symmetry, a lens, disk, or truncated cone has $C_{\infty v}$ symmetry. Strain is taken into account by continuum elasticity, or neglected. Piezoelectricity is neglected. This is the approach taken by classical effective mass[13] or $\mathbf{k}\cdot\mathbf{p}$[9–11] approaches.

Level 2: The nanostructure is constructed from atoms and has therefore C_{2v} symmetry. In this level, however, InAs dot and the GaAs matrix both have the lattice positions of perfect zincblende GaAs. Piezoelectricity is neglected.

Level 3: The atomic positions are relaxed via the valence force field[27] method. Piezoelectricity is neglected.

Level 4: The atomistic structure is relaxed and the piezoelectric effect is included.

By comparing *Level 2* with *Level 1* we capture the effect of atomistic symmetry alone, free from relaxation and piezoelectric effects. By comparing *Level 3* with *Level 2* we capture the effect of atomic relaxation, free from piezoeffect. Finally by comparing *Level 4* with *Level 3*, we capture the effect of piezoelectricity. While other sequences of comparison are possible, we find that this one is the most revealing.

A. Atomistic interface effects: Level 2 versus Level 1

When the atomic positions are assumed to be unrelaxed and piezoelectricity is neglected, the splitting of the electron P states is introduced just by the microscopic symmetry of the interface between the dot material (InAs) and the surrounding material (GaAs). Figure 2 illustrates this effect, where the atomic structure of the different facets $(\bar{1}01)$, (011), (101), $(01\bar{1})$, and (001) (interface 1,2,3,4,5, respec-

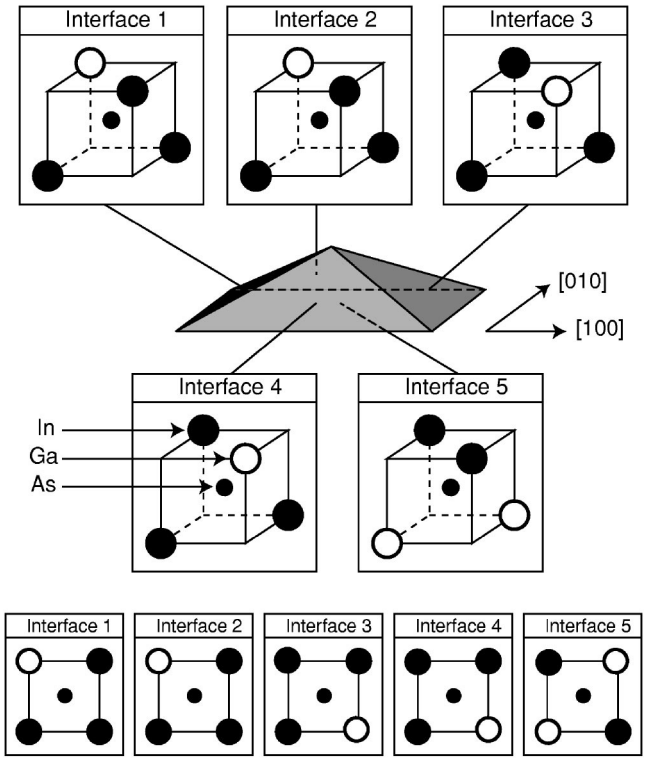

FIG. 2. Atomistic detail of the interfaces of a square-based InAs pyramid with base b and height $b/2$, embedded in GaAs. The zinc-blende unit cells give the atomic arrangement in the direct vicinity of the interface. At the bottom of the figure a top view of the interfaces is given.

tively) of a square-based pyramid are analyzed. For the (001) interface at the base of the pyramid (Fig. 2 interface 5) the [110] and [1$\bar{1}$0] directions are inequivalent. Even for a common anion quantum dot/barrier nanostructure (e.g., InAs/GaAs) the anion plane at interface 5 is anisotropic. The direct neighbors *above* the anion plane (In atoms) that align in the [$\bar{1}$10] direction are chemically different from the neighbors *under* the anion plane (Ga atoms) that align in the [110] direction. Similar observations can be made for all facets of the pyramid and most relevant is the fact that these effects do not compensate each other. At the bottom of Fig. 2 a top view of the zinc-blende unit cells shows that even after the summation of the 1–4 interfaces a net anisotropy remains at the As site.

The effect of the atomistic interface symmetry on the potential of Eq. (1) can be seen in Fig. 3(a) which shows the difference between the pseudopotential $\Sigma_\alpha v_\alpha(\mathbf{r}-\mathbf{R}_\alpha)$ along the [110] and [1$\bar{1}$0] directions for an *unrelaxed* square-based pyramid without piezoeffect. The potential has been averaged in [001] direction over two unit cells centered 1 nm above the base of the pyramid.[64] Figure 3(a) shows that the differences between the atomic pseudopotentials in [110] and [1$\bar{1}$0] directions are well localized at the interfaces (shown as shaded areas marked InGaAs) and vanishes inside the nanostructure.

The first line in Table I shows the magnitude of the atomistic interface effect on the P-level splitting for different shapes and sizes (see Fig. 1 to visualize the geometries). We

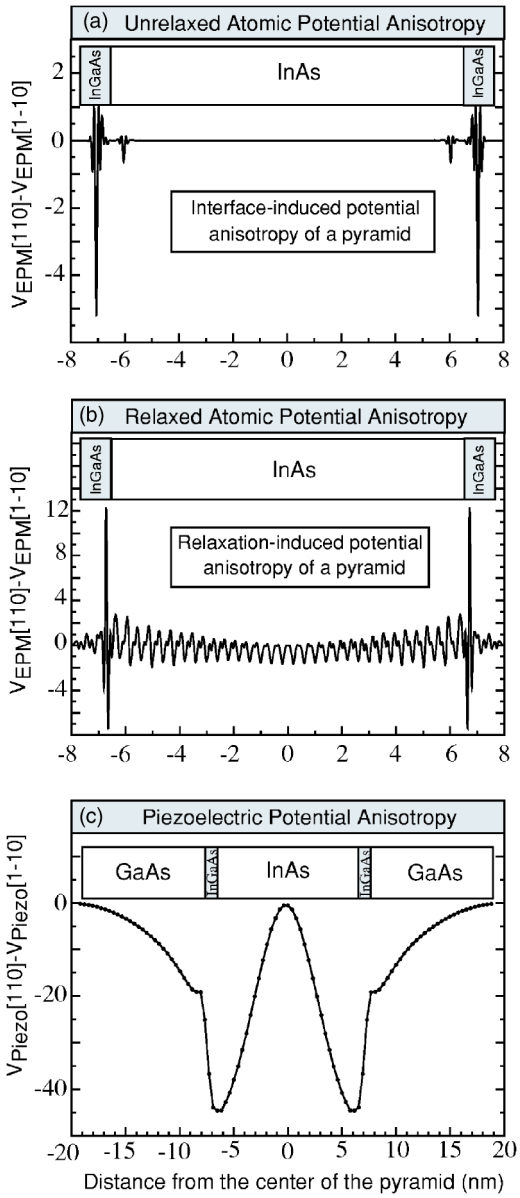

FIG. 3. (a) Difference between the atomistic pseudopotential in [110] and [1$\bar{1}$0] directions for an *unrelaxed* square-based pyramid with 11.3 nm base and 5.6 nm height. The potential has been averaged in [001] direction over two unit cells centered 1 nm above the base of the pyramid. The position of the interfaces are shown as shaded areas labeled InGaAs. (b) Same as (a) for the *relaxed* square-based pyramid. (c) Difference between the piezoelectric potential [using the bulk values of $e_{14}(\mathrm{InAs})=-0.045\ \mathrm{C/m^2}$ and $e_{14}(\mathrm{GaAs})=-0.16\ \mathrm{C/m^2}$] in [110] and [1$\bar{1}$0] directions for the relaxed square-based pyramid.

see in Table I that the interface effect is strongest for the pyramid, having sharply defined facets; this effect splits the electron P states by 3.9 meV. For a truncated cone where the only sharp interfaces are the base and the top, the splitting is smaller, but still 2.3 meV. The two large lenses have a small splitting of 0.5 and 0.4 meV which could be attributed to the fact that the confined states make less "contact" with the interface in a larger structure. The disk has small splitting of 0.1 meV for symmetry reasons: with no vertical facets but

TABLE I. Energy splitting of the electron P states $\Delta E=\varepsilon_{[110]}-\varepsilon_{[1\bar{1}0]}$ where $\varepsilon_{[110]}$ ($\varepsilon_{[1\bar{1}0]}$) is the single particle energy of the electron state oriented along the [110] ([$1\bar{1}0$]) directions in millielectron volts (meV). The contribution "interface" is the difference between *Level 1* (no splitting) and *Level 2* splittings. "Strain" is the difference between *Level 2* and *Level 3* splittings. "Piezo" is the difference between *Level 3* and *Level 4* splittings. The orientation of the first electron P states is given as [iso], for no particular orientation, and as [110] and [$1\bar{1}0$] for the corresponding crystallographic directions. The dimensions of the base b and height h are given in nanometers (nm). The lenses with 25.2 nm base are the most realistic according to Refs. 3 and 4.

	Disk		Lens 1		Truncated cone		Pyramid		Lens 2		Lens 3	
	$b=11.3$,	$h=4.6$	$b=11.3$,	$h=4.6$	$b=11.3$,	$h=5.6$	$b=11.3$,	$h=4.6$	$b=25.2$,	$h=5.5$	$b=25.2$,	$h=3.5$
Interface	0.1	[iso]	2.0	[$1\bar{1}0$]	2.3	[$1\bar{1}0$]	3.9	[$1\bar{1}0$]	0.5	[$1\bar{1}0$]	0.4	[$1\bar{1}0$]
Strain	0.0	[iso]	8.3	[$1\bar{1}0$]	10.5	[$1\bar{1}0$]	18.3	[$1\bar{1}0$]	2.3	[$1\bar{1}0$]	2.2	[$1\bar{1}0$]
Piezo	0.1	[iso]	−4.7	[110]	−4.4	[110]	−8.4	[110]	−5.7	[110]	−3.1	[110]
Total	0.2	[iso]	5.0	[$1\bar{1}0$]	8.4	[$1\bar{1}0$]	13.8	[$1\bar{1}0$]	−2.9	[110]	−0.5	[110]

with two (001) interfaces the effects from both interfaces compensate each other and yield wave functions (not shown) isotropic in the (001) plane with D_{2d} symmetry and no splitting of the electron P states. This effect is similar to the one well known for symmetric quantum wells.[47]

The interfacial symmetry affects the wave functions. The envelope functions for the first electron P state of the pyramid, the truncated cone and the lens are oriented along the [$1\bar{1}0$] direction, whereas the *second* state is oriented along the [110] direction. The wave function orientation is given by the sign of ΔE and explicitely denoted in Table I as [110] or [$1\bar{1}0$] or [iso] (isotropic). The interface effect discussed here is not accounted for by *Level 1* theories based on continuum elasticity (e.g., effective mass models)[13] since the symmetry of the continuum mechanical strain tensor in the (001) plane is C_{4v} so the strain components are equal along the [110] and [$1\bar{1}0$] directions. Such theories produce a vanishing splitting of the electron P states.

B. Atomic relaxation effects: Level 3 versus Level 2

When the atoms are allowed to react to the stress present in all lattice-mismatched self-assembled quantum dots, the interface anisotropy propagates into the interior of the nanostructure. This can be seen in Fig. 3(b) where the difference between the relaxed atomistic potential $\Sigma_\alpha v_\alpha(\mathbf{r}-\mathbf{R}_n)$ along [110] and [$1\bar{1}0$] directions is plotted (without piezoelectric effect). The effect of the interface now penetrates the nanostructure and has a net effect inside the pyramid, directly affecting the main confinement volume.

A further effect contributes to the anisotropy: In a dot of typical shape, where the base is larger than the top, there is a gradient in the magnitude of the strain tensor between top and bottom. Figure 4 shows this gradient for the hydrostatic strain (the trace of the strain tensor) of a pyramidal quantum dot. Each anion in the dot has two cation neighbors above, oriented along the [110] direction, and two cation neighbors below, oriented along the [$1\bar{1}0$] direction. The cations above (along [110]) experience therefore systematically more stress than the cations below (along [$1\bar{1}0$]) making these directions inequivalent.

The magnitude of the stress relaxation effects on the P-level splitting can be seen in the second line of Table I for different dot shapes. For the pyramid, with strong interface anisotropy and the largest height, the atomic relaxation effect is the strongest being 18.3 meV. For the disk, where strain gradient an interface anisotropy are absent, this effect is zero. The truncated cone exhibits also a noticeable splitting of 10.5 meV similar to lens 1 while lens 2 and lens 3 shows a splitting of 2.3 and 2.2 meV, respectively. These results follow the trends calculated for the interface effect. This leads to the interpretation that stress relaxation brings the anisotropy effect well inside the nanostructure where the confined state have largest amplitude.

The top part of Fig. 5 shows for lens shape dot (No. 3) the square of the single particle wave functions for the first nine electron and first nine hole states of the atomistically relaxed structure without piezoelectric potential. The orientation of the electron P states (e_1 and e_2) is along the [$1\bar{1}0$] direction for the first electron P state, and along [110] for the second (upper left part of Fig. 5). For each single particle state, the percentage of the dominant angular momentum component is given in parenthesis. We see that at this level of theory, including atomistic potential and relaxation, the band mixing and angular momentum character mixing is already present. In fact, even the electron states that are often modeled by level-1 single band effective mass theories as a 100% pure states have, in a level 2 theory only around 85% S(levels e_0, e_5), 85% P(levels e_1,e_2,e_8), 80% D(levels e_3,e_4), and 80% F(levels e_6,e_7) character. The hole states h_4 to h_8 exhibit even higher degree of mixing and cannot be modeled, even qualitatively, by a single-band approach.

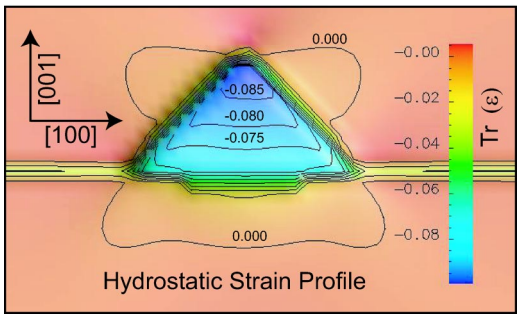

FIG. 4. (Color online) Contour plot of the hydrostatic strain $\boldsymbol{Tr\epsilon}$ for a square-based pyramid with 11.3 nm base and 5.6 nm height. The color bar gives the values of $\boldsymbol{Tr\varepsilon}$.

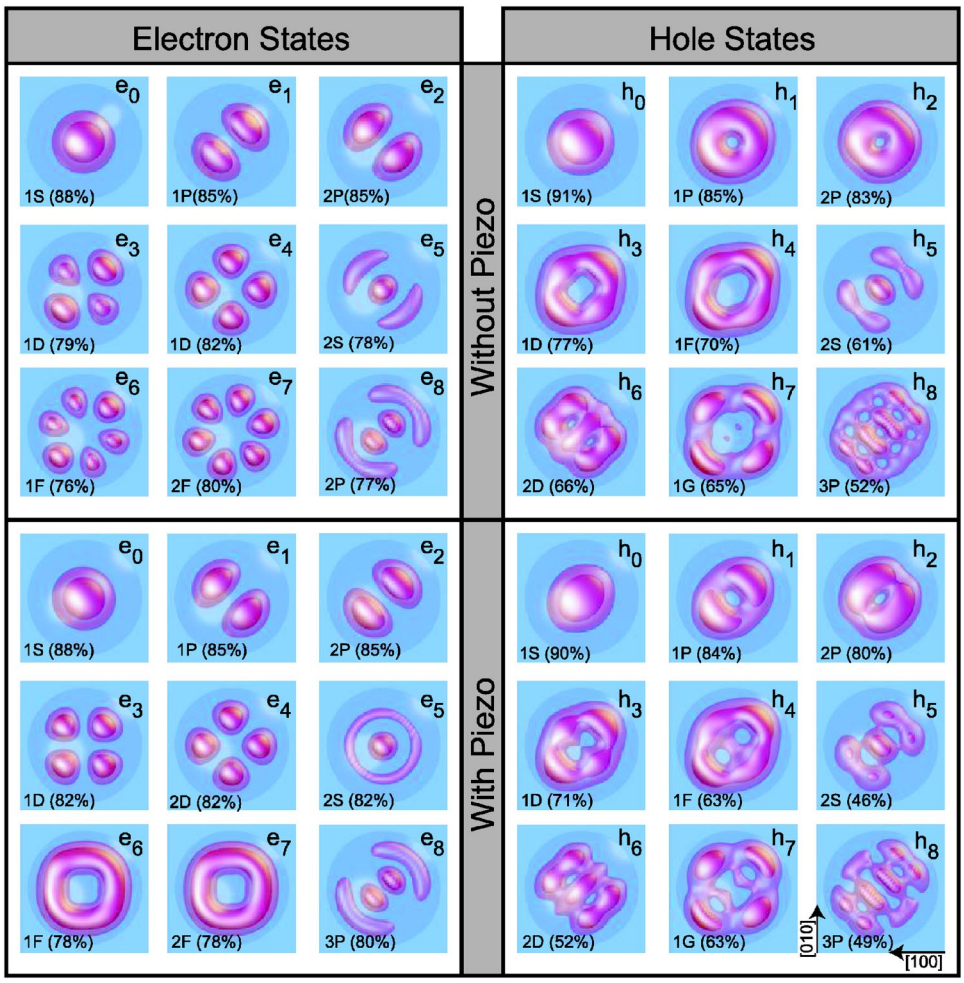

FIG. 5. (Color online) Single-particle electron and hole wave functions squared for a lens shaped InAs/GaAs with 3.5 nm height and 25.2 nm base (lens 3) calculated without piezoelectric effect (upper panel) and with piezoelectric effect (lower part) using $e_{14}(\mathrm{InAs}) = -0.045\ \mathrm{C/m^2}$ and $e_{14}(\mathrm{GaAs}) = -0.16\ \mathrm{C/m^2}$. The isosurface encloses 75% of the state density. The single particle states are labeled (e_0, e_1, …) according to their energy starting with the lowest (highest) energy for electrons (holes). The results of the angular symmetry analysis is given in the lower left corner of each states. The definition of the [010] and [100]-directions is given in the lower right corner of the figure.

The top panels of Fig. 6 show the equivalent of Fig. 5 for the pyramidal quantum dot. The orientation of the electron P states is the same as for the lens: the first electron P state is oriented along the $[1\bar{1}0]$ and the second state along [110]. The first two hole states are oriented along the $[1\bar{1}0]$ direction while the third state is mainly oriented along [110]. The second and third hole states h_1 and h_2 have some occupation probability at the tip of the pyramid which is a consequence of the high strain present in that region. The pyramidal shape is, however, far from the experimental reality.

C. Piezoelectric effect: Level 4 versus Level 3

Strain along the [111] direction in heterovalent zincblende materials gives rise to piezoelectricity.[40] The magnitude of the piezoelectric effect on nanostructures depends on the value of e_{14}. The measured values[43] for the *unstrained* bulk binaries are $e_{14}(\mathrm{InAs}) = -0.045\ \mathrm{C/m^2}$ and $e_{14}(\mathrm{GaAs}) = -0.16\ \mathrm{C/m^2}$. In general, e_{14} changes with strain and composition, as recently demonstrated by several authors[48–56] for (111) grown $\mathrm{In}_x\mathrm{Ga}_{1-x}\mathrm{As/GaAs}$ strained quantum wells. The results of Cho *et al.* are shown in Fig. 7 as solid circles and deviate substantially from the linear, composition-weighted value deduced from the unstrained binaries (dashed line). For a 21% alloy for example, $e_{14} = -0.05\ \mathrm{C/m^2}$, whereas the linearly extrapolated value is $e_{14} = -0.14\ \mathrm{C/m^2}$. Figure 8 shows the number of eight atom unit cells as a function of the off-diagonal strain components ε_{xy}, ε_{yz}, ε_{zx} in a lens-shaped InAs dot embedded in GaAs (two million atoms in total). The inset Fig. 8(b) shows in detail the region of highest strain, revealing that a substantial number of unit cells are highly strained. So in principle, one should use the *strained* value of e_{14} or higher order piezoelectric coefficients to compute the piezoelectric field. Unfortunately no measured or calculated values of piezoelectric coefficients are available for pure but strained InAs. Using the value $e_{14}(\mathrm{InAs}) = -0.045\ \mathrm{C/m^2}$ of the *unstrained* material is almost certainly not relevant for the strained versions of an InAs dot shown in Fig. 8, although previously such values were used to model

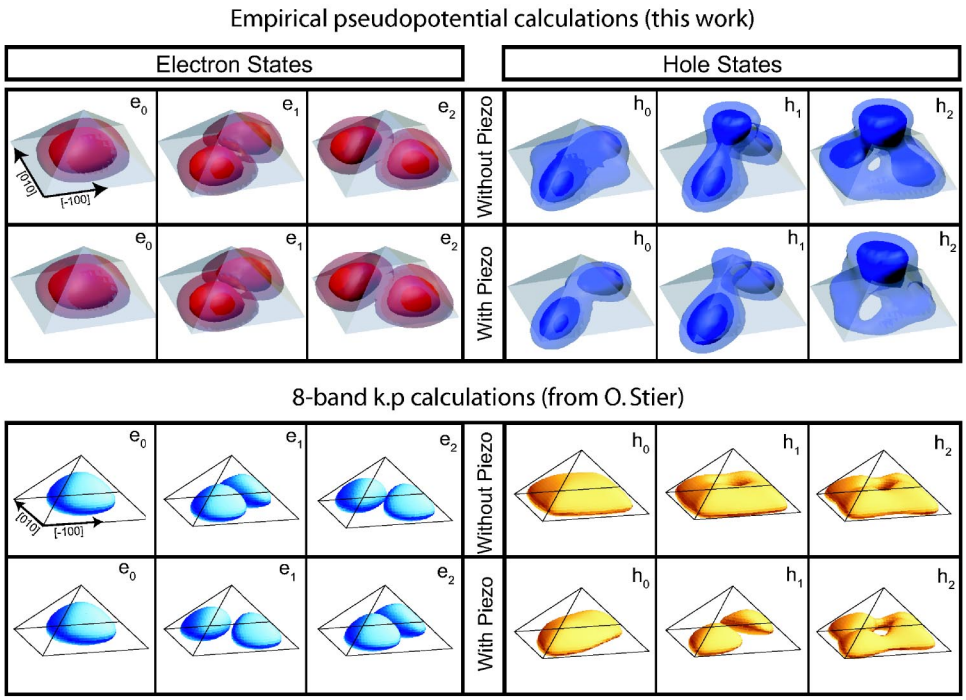

FIG. 6. (Color online) First three single-particle electron and hole wave functions squared for a pyramidal InAs/GaAs quantum dot (11.3 nm base and 5.6 nm height) calculated atomistically with the empirical pseudopotential method and with the eight-band $\mathbf{k}\cdot\mathbf{p}$ method, with (upper panels) and without (lower panels) piezoelectricity. The eight-band $\mathbf{k}\cdot\mathbf{p}$ results are reproductions from Stier.[31] All calculations done with piezoelectricity used $e_{14}(\mathrm{InAs})=-0.045\ \mathrm{C/m^2}$ and $e_{14}(\mathrm{GaAs})=-0.16\ \mathrm{C/m^2}$. The two isosurface for the empirical pseudopotential results enclose 75% and 45% of the state density. The single particle states are labeled (e_0, e_1, …) according to their energy starting with the lowest (highest) energy for electrons (holes). Note that piezoelectricity rotates the lobes of e_1 and e_2 only the $\mathbf{k}\cdot\mathbf{p}$ approximation.

the piezoelectric effect in dots.[22,24,25,57] Thus, in what follows we will first assume the piezoelectric constant of InAs to be the one of the bulk and then, examine the piezoelectric effect using a *range* of InAs e_{14} values.

Figure 3(c) shows the difference between the piezoelectric potential $V_{\mathrm{piezo}}(\mathbf{r})$ along the [110] and $[1\bar{1}0]$ directions of the square-based pyramid using the bulk values e_{14}(InAs) and e_{14}(GaAs). A three dimensional plot for the piezoelectric potential with isosurfaces for potential values of $+30$ and -30 mV is given in Fig. 9(a) for a lens shaped quantum dot. The strongest piezoelectric potential is located outside the nanostructure where the piezoelectric constant is largest and near the interface in regions of highest strain. The piezoelectric field in the region where the states are confined, inside the nanostructure, is noticeably weaker than outside. Figure 9(b) shows a contour plot of the piezoelectric potential in the (001) plane, 1 nm above the base of the lens shaped quantum dot. The potential is positive along the $[1\bar{1}0]$ direction, favoring hole localization and negative along the [110] direction, favoring electron localization.

The effect of piezoelectricity on the energy of the electron P states for different dot shapes can be seen in line 3 of Table I. The piezoelectric effect reduces the splitting induced by the interface and the stress relaxation effects. The strongest magnitude of the effect is again observed for the pyramid with a reduction of the splitting by -8.4 meV. For the pyra-

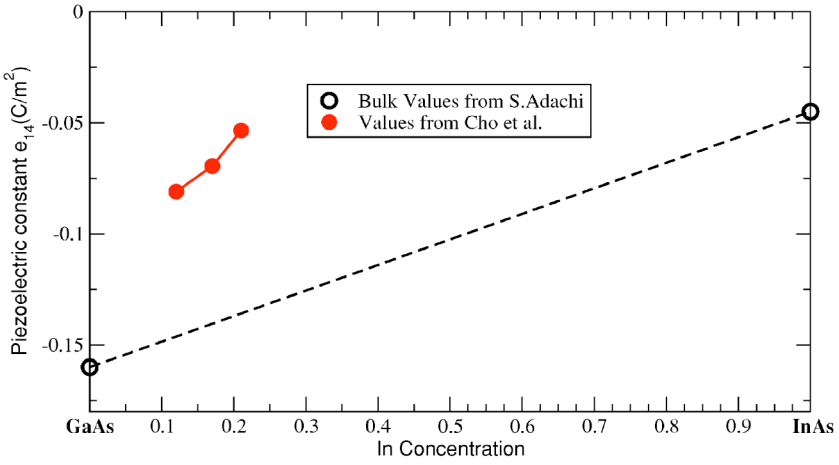

FIG. 7. Composition dependence of the piezoelectric constant e_{14} for a [111] $\mathrm{In}_x\mathrm{Ga}_{1-x}\mathrm{As}$/GaAs quantum well.

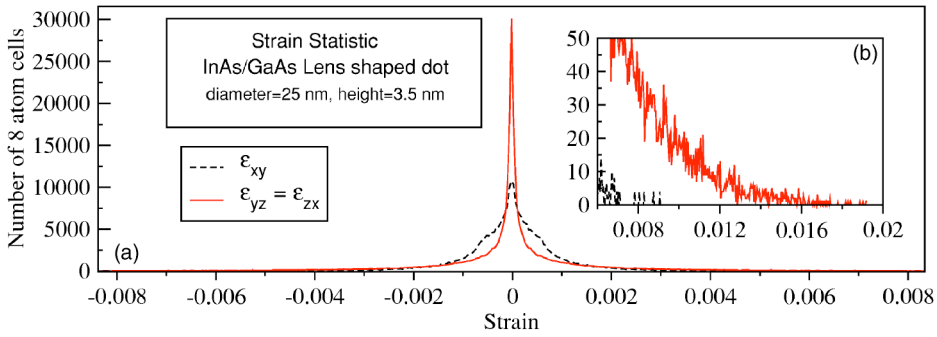

FIG. 8. (a) Strain statistic for the $\epsilon_{xy},\epsilon_{zx},\epsilon_{yz}$ components of the strain tensor, in a lens shaped InAs/GaAs quantum dot with base 25.2 nm and height 3.5 nm. The maximum and minimum values of the strain are $\pm$ 0.0192. The inset (b) shows the tail of the strain distribution.

mid and the truncated cone, piezoelectricity reduces the splitting without changing its sign. For the 5.5 and 3.5 nm tall lenses, however, the piezoelectric effect has larger magnitude than the sum of interface and stress relaxation, and it determines the final orientation of the electron P states. For the most realistic flatter lens of 3.5 nm, the total P-level splitting is -0.5 meV, and the portion due to piezoelectricity is comparable to the one due to interface and stress relaxation.

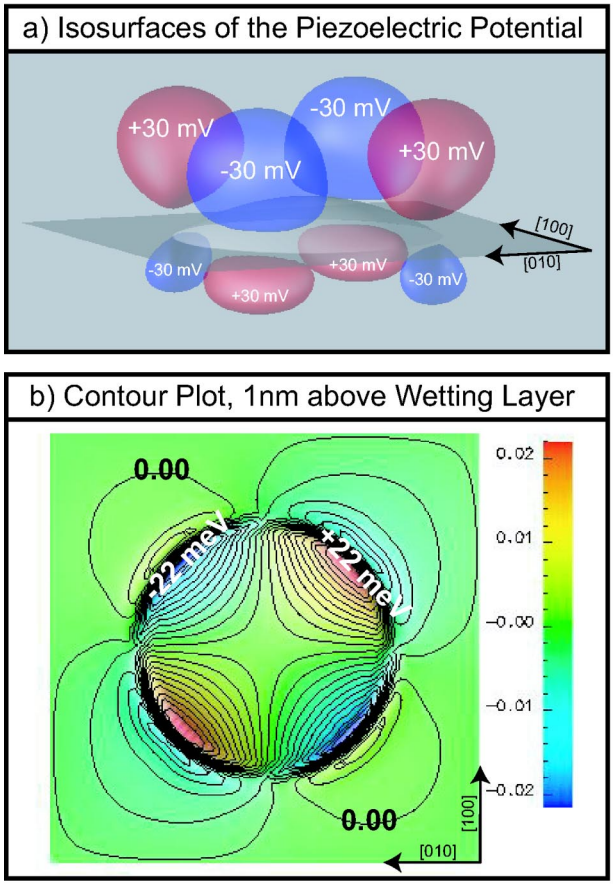

FIG. 9. (Color online) (a) Piezoelectric potential for a lens shape InAs/GaAs quantum dot (base=25.2 nm, height 5 nm). The isosurfaces represent potential values of 30 and -30 mV. The dot and the wetting layer are represented as a gray surface. (b) Contour plot of the piezoelectric potential of the (001) plane 1 nm above the base of the dot.

The effect of piezoelectricity on the wave functions of the flat lens (lens 3) can be seen in the lower half of Fig. 5. In level 4 (with piezoelectricity) the first electron P state e_1 is now oriented along the [110] direction whereas in *Level 3* (without piezoelectricity) it was oriented along the $[1\bar{1}0]$ direction. For the lens shaped dot, the second P-level (e_2) was oriented along the $[1\bar{1}0]$ direction without piezoelectricity but it rotates to the [110] direction when piezoelectricity is considered. In contrast, for the pyramid and the truncated cone the first electron P-state e_1 remain oriented along the $[1\bar{1}0]$ direction in *Level 4* after taking piezoelectricity into account. This can be seen for the pyramid in Fig. 6 that shows the first three electron and hole wave functions squared with and without piezoelectricity. The electron states do not change orientation since the atomistic strain effect of level-2 (that favors $[1\bar{1}0]$ orientation for electrons) is stronger than the piezoelectric effect (that favors [110] orientation). The piezoelectric field makes the orientation of the holes along the [110] direction less favorable. The third hole state h_2 has therefore almost no occupation probability along [110] but mainly towards the apex of the dot.

The percentage of the dominant angular momentum component of each states of the lens is given in Fig. 5 in parenthesis. The effect of piezoelectricity on the angular momentum character is moderate for electron and holes states: the order of the states ($1S$,$1P$,$2P$,etc.) is not affected by piezoelectricity and a maximum deviation of 15% for the state character is observed for h_5. Generally, the character of the hole states is more strongly mixed when piezoelectricity is accounted for. The effect of piezoelectricity is generally stronger on the shape of the envelope functions than on their angular momentum character. Electron (hole) states that are predominantly oriented along the $[1\bar{1}0]$ direction tend to become more (less) isotropic.

As a next step we investigated the dependence of the interface, stress relaxation and piezoelectric effect on the splitting of the electron P states as a function of the height of the dot. Figure 10 shows the splitting ΔE of the electron P states for a lens shape InAs/GaAs with 25.2 nm base and four different heights {3.5,5.0,5.5,6.5} nm. The interface and stress relaxation effects are almost constant as a function of height. The height dependence is however pronounced in *Level 4* taking interface, strain and piezo into account. Flat dots with heights around 3.5 nm have a vanishing splitting of the electron P states while dots with 6.5 nm height have splitting of about 6 meV.

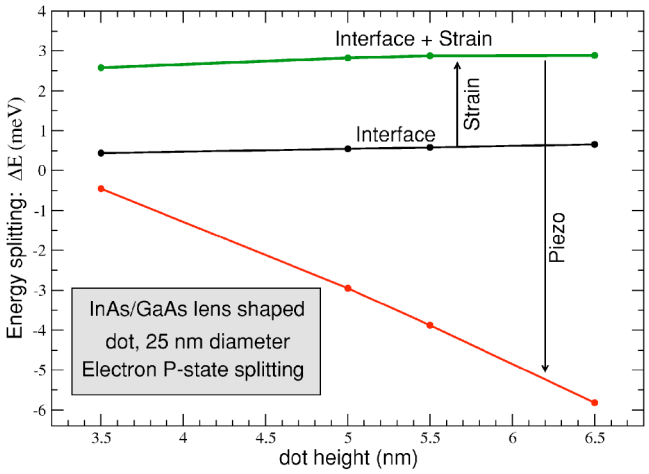

FIG. 10. Height dependence of the splitting of the electron P states, defined as $\Delta E = e_{[110]} - e_{[1\bar{1}0]}$, for the three different levels 2(interface), 3(interface+strain) and 4(interface+strain+piezo) for a lens shape InAs/GaAs dot with 25.2 nm base. We used the bulk InAs and GaAs values of e_{14}.

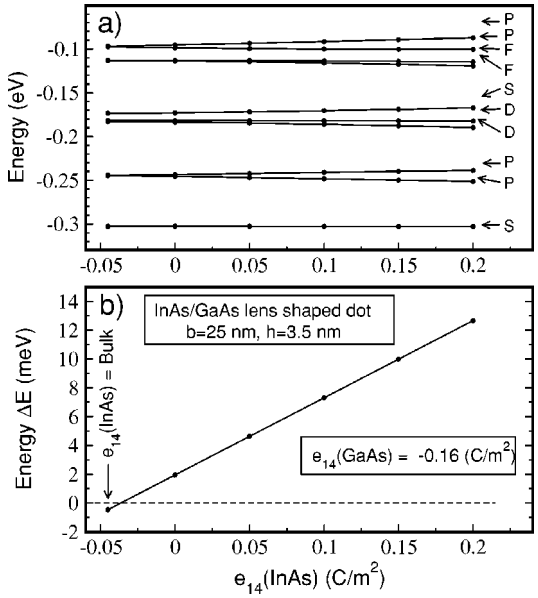

FIG. 11. (a) Eigenvalues of the single-particle electron states for an InAs/GaAs lens shaped dot with 25.2 nm base and 3.5 nm height as a function of e_{14}(InAs). The value of e_{14}(GaAs) is kept constant at the bulk value -0.16 C/m^2. The value of e_{14} for strained InAs is unknown. We give results for an arbitrary range starting from the unstrained InAs value and extending to $+0.2$ C/m^2. The energies are given with respect to the conduction band minimum of bulk GaAs. (b) Energy splitting of the electron P states $\Delta E = e_{[110]} - e_{[1\bar{1}0]}$ for the same dot as in (a).

As noted earlier, the quantum dot is under significant compressive strain (Fig. 8) and the value of the piezoelectric constant e_{14}(InAs) is likely to differ (Fig. 7) from the unstrained bulk value assumed so far. To estimate the effect of the choice of e_{14}(InAs) we performed pseudopotential calculations of the electron states for the following values of e_{14}(InAs) inspired from Fig. 7: $\{-0.045$(bulk value), 0.00,0.05,0.10,0.15,0.20$\}$ C/m^2 (the value of $+0.2$ might be unrealistic). The value of e_{14}(GaAs) is set to the bulk value, which is justified by the fact that the barrier material is mostly unstrained (apart from the interface). The results for the single particle electron eigenvalues for the lens shaped InAs/GaAs dot with 25.2 nm base and 3.5 nm height are plotted in Fig. 11(a). With an increasing value of e_{14}(InAs) the P, D, and F states tend to split further. The dominant orbital character of the levels, in increasing order of energy is S,P,P,D,D,S,F,F,P,P. The P states (e_1,e_2,e_8,e_9) split the most, followed by the D states (e_3,e_4) and the F states (e_6,e_7) that split the least. The S states (e_0,e_5) are nearly independent from the value of e_{14}(InAs). The results for the P states (e_1,e_2) splitting $\Delta E = e_{[110]} - e_{[1\bar{1}0]}$ are plotted in Fig. 11(b). Using the bulk value of e_{14}(InAs)(-0.045 C/m^2[43]) the splitting ΔE is small (-0.5 meV for a lens height of 3.5 nm) and negative, i.e., the fist electron P state is oriented along the [110] direction. When the piezoelectric coefficient e_{14}(InAs) takes on a positive sign the preferred orientation of the electron states is the $[1\bar{1}0]$ direction ($\Delta E > 0$). Figure. 11(b) shows that the splitting of the electron P states is a nearly linear function of the value of e_{14}(InAs) and reaches a maximum of around 13 meV for our largest e_{14}(InAs)$= +0.2$ C/m^2.

IV. COMPARISON WITH PREVIOUS CALCULATIONS

The definition of the crystallographic directions $[1\bar{1}0]$ and [110] depends on the choice of coordinate for the cation atom in the primitive zinc-blende unit cell. We choose to place the cation (Ga) at the origin (0,0,0) and the anion (As) at (1/4,1/4,1/4). This is the conventional orientation of the [111] direction:[43,58,59] from the metallic atom to the nonmetallic atom. Most importantly, this is the convention used by experimentalists when determining the crystallographic directions of a samples using etching techniques.[43]

In order to be able to compare the results from publications where different conventions for the [110] orientation have been used, we apply consistently the definition given earlier to results of Refs. 38 and 60–62. (In some cases, e.g., Ref. 38 mixed definitions were used; these are corrected in Table II). The results are given in Table II, where the available theoretical data on the orientation of the electron and hole P states as well as the energy splitting of the electron P states is given. In Fig. 6 we show the first three electron and hole single particle wave functions for the pyramid calculated with the empirical pseudopotential method (upper panels) and the eight-band $\mathbf{k}\cdot\mathbf{p}$ calculations from Stier.[31] We see that: (i) *No piezoelectricity*: Our results for the pyramid agree with previous EPM results[38,61,62] in wave function orientation and P-level splitting within 10% (see Table II). The $\mathbf{k}\cdot\mathbf{p}$ results of Ref. 31 miss almost entirely the 22 meV splitting of the P level (Table II). In Fig. 6 we see that without piezoelectricity the wave function orientation obtained by the atomistic approach and the $\mathbf{k}\cdot\mathbf{p}$ method are the same for the electron states. For the first three hole states, the $\mathbf{k}\cdot\mathbf{p}$ wave functions are nearly isotropic, while they are anisotropic in the atomistic approach with an orientation along the [110]

TABLE II. Summary of the theoretical results on the orientation of the first electron and hole *P*- states (e_1 and h_1) and the splitting of the electron *P*- states $\Delta E = \varepsilon_{[110]} - \varepsilon_{[1\bar{1}0]}$ in meV. [iso] stands for "isotropic" states without any particular orientation and "…" when the orientation of the state was not reported. The dimensions of the base b and height h of the lens are in nm.

Reference	Method	e_1	h_1	ΔE (meV)
Pyramid (b=11.3 nm, h=5.6 nm), no piezo				
Williamson[38]	EPM	$[1\bar{1}0]$	$[1\bar{1}0]$	26
Wang[61]	EPM	$[1\bar{1}0]$	$[1\bar{1}0]$	24
Kim[62]	EPM	$[1\bar{1}0]$	…	27
Stier[31]	**k·p**	$[1\bar{1}0]$	[iso]	0.3
This work	EPM	$[1\bar{1}0]$	$[1\bar{1}0]$	22.2
Pyramid (b=11.3 nm, h=5.6 nm), with piezo				
Stier[31]	**k·p**	[110]	$[1\bar{1}0]$	−9
This work	**EPM**	**$[1\bar{1}0]$**	**$[1\bar{1}0]$**	**13.8**
Lens 3 (b=25.2, h=3.5), no piezo				
Williamson[38]	EPM	$[1\bar{1}0]$	$[1\bar{1}0]$	2
Shumway[63]	EPM	$[1\bar{1}0]$	[iso]	2
This work	EPM	$[1\bar{1}0]$	$[1\bar{1}0]$	2.6
Lens 3 (b=25.2, h=3.5), with piezo				
This work	**EPM**	**[110]**	**$[1\bar{1}0]$**	**−0.5**

for h_0 and h_1 and mainly at the tip and along the [110] direction for the state h_2. For the lens shape, we agree with previous EPM results[38,63] to within 0.6 meV. Atomistic interface and strain effects favors the $[1\bar{1}0]$ direction for both the electrons and the holes.

(ii) *With piezoelectricity*: Our results for the pyramid disagree with **k·p** in wave function orientation (see Fig. 6) and in *P*-level splitting (13.8 vs −9 meV). Also, in the **k·p** approximation the effect of piezoelectricity is to rotate the e_1 and e_2 wave functions by 90 deg where no such rotation exists in the atomistic approach which gives the correct orientation both, with and without piezoelectric effect. The reason for the disagreement is the missing atomistic splitting of 22 meV in **k·p**. Piezoelectricity favors the [110] direction for electrons and the $[1\bar{1}0]$ direction for holes while atomistic features (levels 2 and 3) favor the $[1\bar{1}0]$ direction for both electrons and holes. For the pyramid the atomistic effects of *levels 2* and *3* prevail and the first electron *P* state is oriented along the $[1\bar{1}0]$. The hole wave function orientation as given by the atomistic and by the **k·p** method agrees for states h_0 and h_1. The state h_2 is partially localized on the tip of the pyramid and partially spread over the base of the pyramid according to the atomistic results, while it is solely spread over the base for the **k·p** results. This difference might be due to the very atomistic character of the highly strained tip which is differently accounted for by atomistic and nonatomistic methods.

For the lens, the piezoelectric effect is stronger than the combined atomistic effects of *levels 2* and *3* and the first electron *P* state is oriented along the [110] direction. The hole *P*- states h_1 have without piezoelectric effect a preference for the $[1\bar{1}0]$ direction and this preference is consolidated by the piezoelectric potential.

V. CONCLUSION

The splitting of the electron *P* states has three distinct origins. First, the atomistic nature of the interface creates an asymmetry in the atomistic potential in the (001) plane. This asymmetry is restricted to the space region close to the interface and only weakly affects the splitting of the localized electron *P*- states $\Delta E = 0$–3.9 meV for different dot shapes. Second, strain relaxation allows for the interface asymmetry to propagate inside the dot, where the states are confined, leading to a further splitting of the *P* states by $\Delta E = 0$–18.3 meV depending on the dot shape (disk versus pyramid). Third, the piezoelectric effect, arising from off-diagonal strain, has the reverse effect on the splitting of electron *P* states with a magnitude of $\Delta E = 0.1$to−8.4 meV. We conclude that neglecting effects 1+2+3 in EMA models is unjustified. Similarly, use of continuum elasticity (neglect of effect 2) is unjustified.

The question has been raised as to whether the use of the bulk piezoelectric constant e_{14} for InAs is justified. Literature suggests that e_{14} might be very different from the bulk value in a strained structure like a quantum dot but has not been reported so far. The calculation or the measurement of the piezoelectric constant e_{14} of strongly strained InAs is called for. The height dependence of the piezoelectric effect on the electron *P*- state splitting is strong with an increase from −0.5 to −6 meV for lens shaped dots of 3.5 – 6.5 nm height. Interestingly, the interface and strain splittings are almost independent on dot height. The effects of interface, strain and piezoelectricity are of comparable magnitude and omitting one might lead to qualitative errors. In particular, previous **k·p** calculations[24] for a pyramidal dot neglecting the atomistic interface and relaxation effects lead to the wrong wave function orientations ([110] instead of $[1\bar{1}0]$) and splittings (−9 meV instead of +13.8 meV).

ACKNOWLEDGMENTS

The authors would like to acknowledge useful communications with O. Stier and D. Bimberg and their kind permission to reproduce the **k·p** wave functions in Fig. 6. They also thank Sergey Dudiy for helpful discussions. This work is supported by the US Department of Energy, Office of Science, Basic Energy Science, Division of Material Science (LAB 3-17 initiative) under Contract No. DEAC36-98-GO10337.

[1] N. Liu, J. Tersoff, O. Baklenov, A. L. Holmes, and C. K. Shih, Phys. Rev. Lett. **84**, 334 (2000).
[2] P. Crozier, M. Catalano, R. Cingolani, and A. Passaseo, Appl. Phys. Lett. **79**, 3170 (2001).
[3] T. Walther, A. G. Cullis, D. J. Norris, and M. Hopkinson, Phys. Rev. Lett. **86**, 2381 (2001).
[4] R. Kegel, T. H. Metzger, A. Lorke, J. Peisl, J. Stangl, G. Bauer, K. Nordlund, W. V. Schoenfeld, and P. M. Petroff, Phys. Rev. B **63**, 035318 (2001).
[5] K. Yamaguchi, Y. Saito, and R. Ohtsubo, Appl. Surf. Sci. **190**, 212 (2002).
[6] D. Bruls, J. Vugs, P. Koenraad, H. Salemink, J. Wolter, M. Hopkinson, M. Skolnick, F. Long, and S. Gill, Appl. Phys. Lett. **81**, 1708 (2002).
[7] U. Woggon, *Optical Properties of Semiconductor Quantum Dots* (Springer-Verlag, Berlin, 1997).
[8] D. Bimberg, M. Grundmann, and N. N. Ledentsov, *Quantum Dots Heterostructures* (Wiley, New York, 1999).
[9] E. O. Kane, *Handbook on Semiconductors* (North Holland, Amsterdam, 1982), Vol. 1.
[10] M. Altarelli, *Band Structure, Impurities and Excitons in Superlattices, Heterojunctions and Semiconductor Superlattices* (Springer, Berlin, 1986).
[11] G. Bastard, *Wave Mechanics Applied to Semiconductor Heterostructures* (Halstead, New York, 1988).
[12] J. Marzin and G. Bastard, Solid State Commun. **92**, 437 (1994).
[13] L. Jacak, P. Harylak, and A. Wójs, *Quantum Dots* (Springer-Verlag, Berlin, 1998).
[14] M. Koskinen, S. M. Reimann, and M. Manninen, Phys. Rev. Lett. **90**, 066802 (2003).
[15] D. Ceperley, Rev. Mod. Phys. **67**, 279 (1995).
[16] M. Sugisaki, H.-W. Ren, S. V. Nair, K. Nishi, S. Sugou, T. Okuno, and Y. Masumoto, Phys. Rev. B **59**, R5300 (1999).
[17] S. Cortez, O. Krebs, P. Voisin, and J. M. Gerard, Phys. Rev. B **63**, 233306 (2001).
[18] G. Cantele, G. Piacente, D. Ninno, and G. Iadonisi, Phys. Rev. B **66**, 113308 (2002).
[19] K. Silverman, R. Mirin, S. Cundiff, and A. Norman, Appl. Phys. Lett. **82**, 4552 (2003).
[20] A. S. Saada, *Elasticity: Theory and Applications* (Pergamon Press, New York, 1974).
[21] C. Pryor, J. Kim, L.-W. Wang, A. J. Williamson, and A. Zunger, J. Appl. Phys. **83**, 2548 (1998).
[22] M. Grundmann, O. Stier, and D. Bimberg, Phys. Rev. B **52**, 11969 (1995).
[23] *Nano-Optoelectronics Concepts, Physics and Devices*, edited by M. Grundmann, (Springer, Berlin, 2002), Chap. 7.
[24] O. Stier, M. Grundmann, and D. Bimberg, Phys. Rev. B **59**, 5688 (1999).
[25] G. Pryor, Phys. Rev. B **57**, 7190 (1998).
[26] S. Hackenbuchner, M. Sabathil, J. Majewski, G. Zandler, P. Vogl, E. Beham, A. Zrenner, and P. Lugli, Physica B **314**, 145 (2002).
[27] P. N. Keating, Phys. Rev. **145**, 637 (1966).
[28] S. J. Jiang, Phys. Rev. B **56**, 4696 (1997).
[29] M. Cusack, P. Briddon, and M. Jaros, Phys. Rev. B **54**, R2300 (1996).
[30] T. Bahder, Phys. Rev. B **41**, 11992 (1990).
[31] O. Stier, *Electronic an Optical Properties of Quantum Dots and Wires* (Wissenschaft & Technik Verlag, Berlin, 2001).
[32] A. Zunger, Phys. Status Solidi B **224**, 727 (2001).
[33] R. Santoprete, B. Koiller, R. Capaz, P. Kratzer, Q. Liu, and M. Scheffler, Phys. Rev. B **68**, 235311 (2003).
[34] Y. Niquet, C. Delerue, G. Allan, and M. Lannoo, Phys. Rev. B **62**, 5109 (2000).
[35] G. Klimeck, F. Oyafuso, T. B. Boykin, R. Bowen, and P. von Allmen, Comput. Model. Eng. Sci. **3**, 601 (2002).
[36] V. Ranjan, G. Allan, C. Priester, and C. Delerue, Phys. Rev. B **68**, 115305 (2003).
[37] G. Bryant and W. Jaskolski, Phys. Rev. B **67**, 205320 (2003).
[38] A. J. Williamson, L.-W. Wang, and A. Zunger, Phys. Rev. B **62**, 12963 (2000).
[39] A. J. Williamson and A. Zunger, Phys. Rev. B **59**, 15819 (1999).
[40] R. Martin, Phys. Rev. B **5**, 1607 (1972).
[41] R. Resta, Rev. Mod. Phys. **66**, 899 (1994).
[42] N. Marzari and D. Vanerbilt, Phys. Rev. B **56**, 12847 (2002).
[43] S. Adachi, *Physical Properties of III–V Semiconductor Compounds* (Wiley, New York, 1992).
[44] W. H. Press, S. A. Teukolsky, W. T. Vetterling, and B. P. Flannery, *Numerical Recipes* (Cambridge University Press, Cambridge, 1992).
[45] L.-W. Wang and A. Zunger, Phys. Rev. B **59**, 15806 (1999).
[46] L. W. Wang, A. J. Williamson, A. Zunger, H. Jiang, and J. Singh, Appl. Phys. Lett. **76**, 339 (2000).
[47] S. Cortez, O. Krebs, and P. Voisin, J. Vac. Sci. Technol. B **18**, 2232 (2000).
[48] S. Cho, J. Kim, A. Sanz-Hervas, A. Majerfeld, G. Patriarche, and B. Kim, Phys. Status Solidi A **195**, 260 (2003).
[49] P. Ballet, P. Disseix, J. Leymarie, A. Vasson, A.-M. Vasson, and R. Grey, Thin Solid Films **336**, 354 (1998).
[50] C. H. Chan, M. C. Chen, H. H. Lin, Y. F. Chen, G. J. Jan, and Y. H. Chen, Appl. Phys. Lett. **72**, 1208 (1998).
[51] P. D. Berger, C. Bru, Y. Baltagi, T. Benyattou, M. Berenguer, G. Guillot, X. Marcadet, and J. Nagle, Microelectron. J. **26**, 827 (1995).
[52] J. L. Sanchezrojas, A. Sacedon, F. Gonzalezsanz, E. Calleja, and E. Munoz, Appl. Phys. Lett. **65**, 2042 (1994).
[53] T. B. Bahder, R. L. Tober, and J. D. Bruno, Phys. Rev. B **50**, 2731 (1994).
[54] R. L. Tober and T. B. Bahder, Appl. Phys. Lett. **63**, 2369 (1993).
[55] R. A. Hogg, T. A. Fisher, A. R. K. Willcox, D. M. Whittaker, M. S. Skolnick, D. J. Mowbray, J. P. R. David, A. S. Pabla, G. J. Rees, R. Grey, *et al.*, Phys. Rev. B **48**, 8491 (1993).
[56] A. S. Pabla, J. L. Sanchezrojas, J. Woodhead, R. Grey, J. P. R. David, G. J. Rees, G. Hill, M. A. Pate, P. N. Robson, R. A. Hogg, *et al.*, Appl. Phys. Lett. **63**, 752 (1993).
[57] M. A. Migliorato, A. G. Cullis, M. Fearn, and J. H. Jefferson, Physica E (Amsterdam) **13**, 1147 (2002).
[58] P. Yu and M. Cardona, *Fundamentals of Semiconductors* (Springer, Berlin, 2001).
[59] A. Zunger and S. Mahajan, *Handbook on Semiconductors* (Elsevier Science B.V., Amsterdam, 1994), Vol. 3, Chap. 19.
[60] L.-W. Wang, J. Kim, and A. Zunger, Phys. Rev. B **59**, 5678 (1999).
[61] L. Wang, A. Williamson, A. Zunger, H. Jiang, and J. Singh, Appl. Phys. Lett. **76**, 339 (2000).

[62] J. Kim, L.-W. Wang, and A. Zunger, Phys. Rev. B **57**, R9408 (1997).

[63] J. Shumway, A. J. Williamson, A. Zunger, A. Passaseo, M. DeGiorgi, R. Cingolani, M. Catalano, and P. Crozier, Phys. Rev. B **64**, 125302 (2001).

[64] This averaging procedure is necessary since the zinc-blende lattice is intrinsically anisotropic within one unit cell. This anisotropy is not the one responsible for the splitting of the *P* states in the nanostructure, and we eliminate it by taking an average over an integer number of unit cells.